Study of stratospheric air density irregularities based on two-wavelength observation of stellar scintillation by Global Ozone Monitoring by Occultation of Stars (GOMOS) on Envisat

A.-S. Gurvich, Francis Dalaudier, Viktoria F. Sofieva

Study of stratospheric air density irregularities based on two-wavelength observation of stellar scintillation by Global Ozone Monitoring by Occultation of Stars (GOMOS) on Envisat

A. S. Gurvich
A. M. Oboukhov Institute of Atmospheric Physics, Moscow, Russia

F. Dalaudier
Service d'Aeronomie, Paris, France

V. F. Sofieva
Finnish Meteorological Institute, Helsinki, Finland

Received 21 October 2004; revised 24 February 2005; accepted 18 March 2005; published 14 June 2005.

[1] The scintillations of stars observed through the Earth's atmosphere are generated by random irregularities of air density. We propose the qualitative theory for description of coherency and correlations of optical scintillations measured at two wavelengths. It is based on a two-component model of air density irregularities: One of the components corresponds to anisotropic irregularities, while the second one is generated by locally isotropic turbulence. The main conclusion of the developed theory is that chromatic aberration results in low coherency of isotropic scintillations. The scintillations measured by GOMOS fast photometers (FP) on board the Envisat satellite have confirmed the theoretical conclusions. The coherency of scintillation measurements at wavelength 672 and 499 nm visualize the regions of high coherency where the anisotropic irregularities dominate. Observations have allowed also the detection of layers with low coherence. They are located generally between altitudes of 30 and 40 km. The thickness of the layers and their altitude distribution depend on observation location. It is expected that the locally isotropic turbulence is strongly developed within these layers. We show that the low values of the cross-correlation coefficient of two-wavelength scintillations can be used as a qualitative indicator for the presence of layers with prevailing isotropic turbulence. The obtained results showed that the analysis of two-wavelength coherency and cross-correlation functions is a sensitive approach which will allow visualizing IGW breakdown in the stratosphere.

Citation: Gurvich, A. S., F. Dalaudier, and V. F. Sofieva (2005), Study of stratospheric air density irregularities based on two-wavelength observation of stellar scintillation by Global Ozone Monitoring by Occultation of Stars (GOMOS) on Envisat, *J. Geophys. Res.*, *110*, D11110, doi:10.1029/2004JD005536.

1. Introduction

[2] Investigation of density and composition of planetary atmospheres originated from ground-based observations of stellar occultations by planets [*Elliot and Veverka*, 1976; *Hubbard et al.*, 1993]. Exploitation of satellites makes it possible to apply a similar approach in studying the Earth's atmosphere. It is well known that stellar scintillation is a consequence of diffraction of light on air density (and, consequently, refractive index) irregularities. Such irregularities appear in the atmosphere because of turbulence and internal waves. Parameters of internal waves and turbulence in the Earth's atmosphere were estimated from space observations of stellar scintillation [*Gurvich*, 2002; *Gurvich and Kan*, 2003a, 2003b; *Gurvich and Chunchuzov*, 2003, 2005]. Scintillation measurements performed simultaneously at two wavelengths by GOMOS fast photometers (FP) on board the Envisat satellite [*Kyrölä et al.*, 2004] open new possibilities for studying the atmospheric structure based on exploitation of chromatic refraction [*Dalaudier et al.*, 2001; *Kan et al.*, 2001]. Chromatic refraction is a consequence of dependence of refractive index on wavelength. As a result, the rays coming from a star to the observation point do not coincide in the atmosphere, intersecting different irregularities. Therefore the correlation of scintillations at different wavelength decreases with increased separation of rays [*Tatarskii*, 1971].

[3] In the current paper, we consider coherency of synchronous bi-chromatic scintillations and show which information on air density irregularities can be retrieved from such data analysis. The scintillations at two wave-

0148-0227/05/2004JD005536

length λ_B = 499 nm and λ_R = 672 nm recorded by the GOMOS FP are used as experimental data.

2. Qualitative Theory of Scintillations

[4] Three-dimensional (3-D) spatial spectrum of air refractivity determines observed scintillations [*Tatarskii*, 1971]. We present here the qualitative theoretical analysis of the coherency based on two-component model of 3-D spatial spectrum Φ_ν of relative fluctuations of air density (equivalently, refractivity ν) in the stratosphere $\Phi_\nu = \Phi_W + \Phi_K$. This model was already successfully used in order to interpret monochromatic or finite bandwidth scintillation measurements. We give here in short its main characteristics; for further details, see *Gurvich and Brekhovskikh* [2001], *Gurvich and Kan* [2003a], and *Gurvich and Chunchuzov* [2003]. The first component Φ_W corresponds to anisotropic irregularities generated mainly by internal gravity waves (IGW). This component contains two typical wave numbers: large κ_w and small κ_* corresponding to buoyancy scale and outer scale. The associated vertical temperature spectrum is proportional to $C_W^2|\kappa_z|^{-3}$ for $\kappa_w > |\kappa_z| > \kappa_*$. It corresponds to the saturated gravity waves model [*Fritts and VanZandt*,1993]. Parameter C_W^2 characterizes a power of anisotropy irregularities. The anisotropy of the wave component is assumed to be large as confirmed by observations [*Alexandrov et al.*, 1990].

[5] The second component Φ_K corresponds to isotropic irregularities generated by turbulence, which may appear as a result of internal-wave breaking. We accept Kolmogorov's model for Φ_K with its structure characteristics C_K^2. Wave number κ_K corresponds to Kolmogorov's scale, $\kappa_K > \kappa_w$, always. In this way we can consider IGW breaking as an outer source of energy with respect to originating turbulence. It allows us to assume that structure characteristic C_K^2 of an originated turbulence is defined by IGW power C_W^2. At the same time, such consideration allows us to assume that there is no correlation between isotropic and anisotropic irregularities.

[6] During observations of stars through the atmosphere, each component of Φ_ν produces scintillation in the observation plane. As long as the observation is performed in the weak scintillation regime, the spatial 2-D scintillation spectrum F_I is the sum of anisotropic $F_I^{(A)}$ and isotropic $F_I^{(I)}$ components [*Gurvich and Brekhovskikh*, 2001] and there is no correlation between anisotropic and isotropic scintillation. Previous spacecraft observations [*Gurvich and Kan*, 2003a, 2003b; *Gurvich and Chunchuzov*, 2003, 2005] were already analyzed successfully using this two components model in the stratosphere. The results of these monochromatic observations gave some examples of estimations of parameters C_W^2, C_K^2, κ_K, κ_w, κ_* for altitudes 2–70 km.

[7] For this first analysis of two-wavelength observations, we start with qualitative considerations. Using the scintillation records at wavelengths λ_B and λ_R, we calculate 1-D auto-spectra of scintillations V_B and V_R, respectively, along the satellite trajectory. Auto-spectra V_B and V_R are the sums $V_B = V_B^{(A)} + V_B^{(I)}$, $V_R = V_R^{(A)} + V_R^{(I)}$, where the superscripts correspond to anisotropic and isotropic components. The squared coherency Coh(f) is defined by

$$\mathrm{Coh}(f) = |V_{BR}(f)|^2/(V_B(f)V_R(f)), \qquad (1)$$

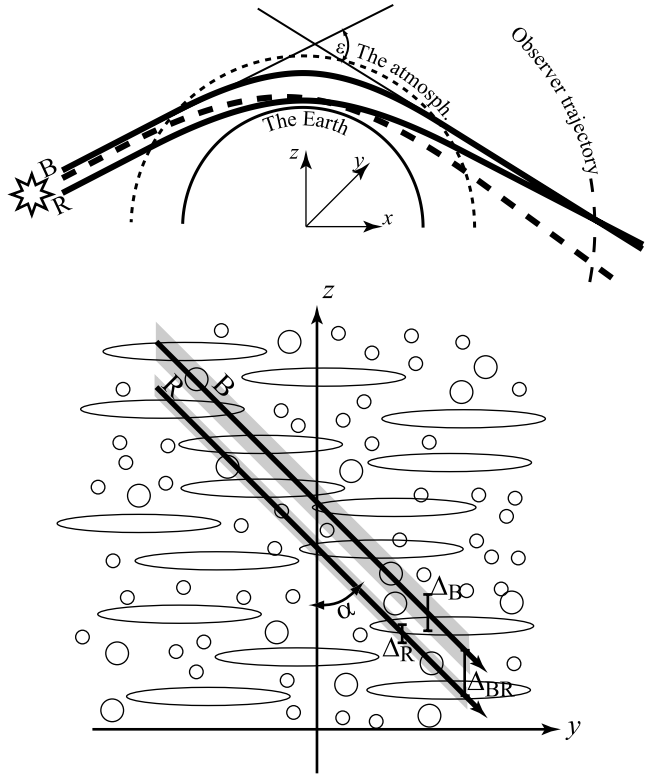

Figure 1. Observation scheme of the two-wavelength scintillation. (top) A cut of the atmosphere by the plane containing B (blue) and R (red) rays (thick solid lines), which are received at the same time t_0 by the FP. The ray curvature and the refraction angle ε are largely exaggerated. Thick dashed line denotes a blue ray having the same ray perigee altitude as the red one, but coming to FP with a refractive time delay δτ. (bottom) A cut of the atmosphere by the atmospheric screen. Solid lines denote trajectories of the intersection points of the rays with this plane. Shading illustrates chromatic "thickness" Δ_R and Δ_B of the rays. The photometers simultaneously register the rays with the same coordinate y. Sketched contours illustrate anisotropic and isotropic irregularities of air density.

where $V_{BR}(f)$ is the cross spectrum of two-wavelength scintillation and f is the frequency. The squared coherency is always smaller than (or equal to) 1. If the scintillations are noncorrelated in some frequency domain, then $V_{BR} = 0$ and Coh = 0. We will use below the term "coherency" instead of "squared coherency," for short.

[8] It is not so difficult to calculate the modeled spectra V_R, V_B, and V_{BR} if the 3-D model of the spatial spectra Φ_ν is known. However, the calculations lead to cumbersome formulae provided that finite wavelength band of optical filters of photometers, refractive dilution, etc. [*Dalaudier et al.*, 2001; *Gurvich and Brekhovskikh*, 2001; *Gurvich et al.*, 2001; *Kan*, 2004] are taken into account. Therefore we consider a simplified model (Figure 1) of spacecraft observations, which helps us to understand important properties of the coherency. The light rays registered by the photometer are bent downward in the atmosphere because of the refraction. These rays are plane curves for a spherically symmetrical atmosphere. The ray plane contains the direc-

tion of the observed star, the Earth's center, and the observer. The real refraction angle ε for both rays is small ($\varepsilon \leq 1.6 \times 10^{-3}$ radian for altitudes above 20 km) but were strongly exaggerated for visualization.

[9] Let us consider the simplest case when Envisat orbit plane coincides with the ray plane. (Figure 1, top). Since the refractive index increases with decreasing wavelength, the ray perigee altitude h_B of the blue ray is always higher than that of the red one h_R. We have $h_B - h_R = \Delta_{BR} > 0$. The change of Δ_{BR} with altitude for GOMOS FP, calculated using U.S. standard atmosphere 1976, is presented in Figure 6 of *Dalaudier et al.* [2001]. Typical values are: $\Delta_{BR} = 0.6 \sim 0.8$ m at altitude 50 km, 6∼9 m at 30 km, and 30∼50 m at 20 km. The heavy dashed line in Figure 1 represents the blue ray with the same perigee altitude as the red one. It reaches the instrument after some time delay [*Kyrölä et al.*, 2004], and its path within the atmosphere does not coincides exactly with the red ray path.

[10] Taking into account the finite band of optical filters, red and blue rays, recorded by the photometer at any given time, should not be thought of as a single curve but rather as two vertical strips contained within the same plane. The height of each strip is proportional to the refractivity band associated with the filter. As a consequence, ray perigee altitudes form non-overlapping bands of depth Δ_R and Δ_B respectively. Using the work by *Dalaudier et al.* [2001], values Δ_R and Δ_B can be estimated as $\Delta_R = 17\%$ and $\Delta_B = 44\%$ of Δ_{BR}, respectively. Typical values of Δ_R and Δ_B are $1.5 \sim 2.0$ m and $4 \sim 5$ m at ray perigee altitude ∼30 km or $5 \sim 8$ m and $13 \sim 22$ m at altitude ∼20 km. Spatial averaging in these vertical strips smoothes the scintillations of the corresponding scales. When the satellite moves, the successive rays move downward within the atmosphere (GOMOS looks only at star settings).

[11] In the general situation, the trajectory of the satellite is not contained within the ray plane, and the displacement of the ray within the atmosphere is no longer vertical. The ray plane revolves on axis directed from the Earth's center to the observed star during an observation. The velocity of ray motion (perpendicular to the ray) depends on the angle between orbit pole and star direction. It is between 3 and 8 km/s so that we can safely apply the frozen field approximation with respect to all atmospheric motions. Figure 1 (bottom) represents a cut of the atmosphere by the plane passing through the Earth's center, and this cut is perpendicular to observed star direction; this is an atmospheric phase screen [*Ishimaru*, 1978]. On the screen, we will employ the reference frame tied to the projection of the Earth on this screen. We will take into account the smallness of ε. The normal z of the Earth's limb is the intersection of ray and screen planes. The y axis on Figure 1 (bottom) is tangent to limb projection in the cross point z and the limb. The normal z revolves around the Earth's center during the observation. The lines R and B correspond to motion of these points. The angle α is the angle between z and the direction of velocity of these points on the screen plane in some observation moment t_0. If an observed star belongs to the orbit plane, then $\alpha = 0$.

[12] For our studies, it is interesting to consider stratospheric irregularities contained within a spherical shell with a thickness equal to the atmospheric scale height H_0. For this reason, we divided the scintillation records into parts for processing. The time duration of parts was $T_0 \approx H_0/V_P$ where V_P is vertical velocity of ray perigee point. We may consider a motion of the normal z during T_0 as translational movement since the atmospheric scale height H_0 is many times less than the Earth's radius. This allows us also to ignore the curvature of the limb for observations during the time T_0, and we use the rectangular coordinates with axes y and z on the screen plane. The contours sketched on Figure 1 (bottom) illustrate isotropic and anisotropic irregularities (strongly elongated along the Earth's surface) of air density. The diffraction of light by these irregularities results in observed scintillation. Shading in Figure 1 shows averaging along Δ_R and Δ_B simplistically. Because the reference frame is fixed with respect to the ground, the (projection of the) Earth's rotation is automatically taken into account, modifying only slightly the value of the angle α.

2.1. Contribution From Isotropic Fluctuations

[13] Let us consider the impact of the isotropic irregularities on the rays simultaneously recorded by the red and blue photometers in the general case $\alpha \neq 0$. We assume that Φ_K corresponds to the Kolmogorov's locally isotropic turbulence. Theory and experiment [*Tatarskii*, 1971] show that the main contribution to scintillation power comes from the scale $\sim \max(l_K, \sqrt{\lambda L})$, where l_K is the inner scale of turbulence and L is the distance from the tangent point to the satellite. The typical values for the stratosphere are $l_K = 0.3 \div 0.7$ m [*Gurvich and Kan*, 2003b] and $\sqrt{\lambda L} = 1.4$ m for GOMOS observations. If the distance $\Delta_{BR} \sin\alpha$ between propagation paths for B and R is larger than $\max(l_K, \sqrt{\lambda L})$, it can be considered that the corresponding rays intersect statistically independent irregularities and, consequently, scintillations at two wavelengths are not very coherent. Otherwise, each ray intersects mostly the same dominant irregularities, and higher coherency is expected. We focus our attention on low frequencies $f < V_S/\max(l_K, \sqrt{\lambda L})$, where V_S is the velocity of the intersection of the ray with the atmospheric screen plane. The 1-D auto-spectra are practically independent of f for these frequencies (flat spectrum). Full calculations [*Kan*, 2004] show that the expected value of coherency is close to 0.4 for the ray perigee 50 km and $\alpha = 30°$, and it is even smaller for $\alpha > 30°$. As ray altitude decreases, Δ_{BR} grows nearly exponentially and the coherency of scintillations generated by isotropic irregularities rapidly drops to zero.

[14] For small values of α: $\sin\alpha \ll \max(l_K, \sqrt{\lambda L})/\Delta_{BR} \equiv \sin\alpha_{\max}$, one would expect high coherency of two-wavelength scintillations. Nevertheless, even in exactly vertical occultation ($\alpha = 0$) the bi-chromatic scintillation cannot be completely correlated because of the following reasons. First, the blue and red rays having the same tangent altitude does not exactly coincide within the atmosphere (Figure 1, top) because of small differences in refractive angles and ray curvature. The effective divergence of rays (∼0.9 m at 30 km) can lead to significant reduction of coherency for bi-chromatic scintillations. Second, if we take into account the Earth's rotation, then blue and red rays cross the same irregularities during a given occultation with given α in only some altitude ranges since the vertical velocity V_P depends on altitude because of refraction. Some numerical estimations of the ray divergence due to chro-

matic effects and Earth's rotation are given in Appendix A. We considered Kolmogorov's spectrum as an example. Qualitative results of the above consideration would hold for all locally isotropic spectra with power law 3-D spectrum [*Tatarskii*, 1971].

2.2. Contribution From Anisotropic Fluctuations

[15] The measurements [*Gurvich and Chunchuzov*, 2003, 2005; *Gurvich and Kan*, 2003b] have shown that the minimal vertical scale of anisotropic irregularities is larger than a few meters for $h > 20$ km. It means that these irregularities originate scintillations by means of focusing/defocusing in the main. The anisotropic irregularities are strongly elongated in the horizontal direction because of influence of buoyancy forces. The ratio of their horizontal and vertical scales seems to be larger than 15–30. If the value $|\pi/2 - \alpha|$ is not very small, then blue and red rays intersect practically the same irregularities with some time delay τ_A [*Kyrölä et al.*, 2004] $\tau_A = \Delta_{BR}/V_S \cos\alpha$. It is true on condition that $\cos\alpha > 1/\eta$. The time delay does not affect the values of the coherency. Therefore we may assume the coherency of anisotropic scintillations is defined mainly by instrumental noise and is expected to be close to 1 for bright stars.

2.3. Combined Contributions

[16] Now we can analyze equation (1), taking into account that we can obtain only a combination of anisotropic and isotropic auto- and cross-spectra from measurements. The anisotropic scintillations can be well described with geometric optics approximation; therefore $V_R^{(A)} = V_B^{(A)} = V^{(A)}$ [*Gurvich and Brekhovskikh*, 2001]. This equation is true when it is possible to ignore chromatic spatial averaging. However, the influence of this averaging on the coherency is very weak for $|\alpha| < 83 \div 85°$ [*Kan*, 2004]. Hence the cross-spectrum of the anisotropic component is

$$V_{BR}^{(A)}(f) = V^{(A)}(f)\exp(i2\pi f\tau_A). \tag{2}$$

[17] In the case of the Kolmogorov's spectrum Φ_K we can consider that the 1-D spectral density of scintillation does not depend on f at low frequencies. This allows us to estimate the ratio $V_B^{(I)}(f)/V_R^{(I)}(f)$ of spectral densities by $1 \le V_B^{(I)}(f)/V_R^{(I)}(f) \le (\lambda_R/\lambda_B)^{7/6} = 1.44$. The lower and upper bounds in these inequalities correspond to $l_K \gg \sqrt{\lambda L}$ or $l_K \ll \sqrt{\lambda L}$ [*Tatarskii*, 1971]. Note that the distortion of the scintillation spectrum because of the finite wavelength band of optical filters is not taken into account in the above inequalities. The ratio $V_B^{(I)}/V_R^{(I)}(f)$ can be slightly less than 1 due to this reason, but it remains independent of frequency f. The cross-spectrum $V_{BR}^{(I)}(f)$ of isotropic irregularities can only be described as

$$V_{BR}^{(I)} = \sqrt{\mathrm{Coh}^{(I)}}V^{(I)}\exp(i2\pi f\tau_I), \tag{3}$$

where $\mathrm{Coh}^{(I)}$ is the coherency of scintillations generated by isotropic irregularities of the refractive index, $V^{(I)} = \sqrt{V_B^{(I)}V_R^{(I)}}$, and $\tau_I = \Delta_{BR}\cos\alpha/V_S$ is the time delay corresponding to the minimal distance between red and blue trajectories. Detailed study of $V_{BR}^{(I)}(f)$ is given by *Kan* [2004].

[18] The coherency (1) can be estimated, taking into account that $V_R^{(I)} \approx V^{(I)}$ and $V_B^{(I)} \approx V^{(I)}$ for low frequencies. Then, after simple transformations, we get

$$|V_{BR}|^2 = \left(V^{(I)}\right)^2\mathrm{Coh}^{(I)} + \left(V^{(A)}\right)^2 + 2V^{(I)}V^{(A)}\sqrt{\mathrm{Coh}^{(I)}}\cos(2\pi f(\tau_A - \tau_I)). \tag{4}$$

Substituting (4) into (1), we get the theoretical estimate of the coherency,

$$\mathrm{Coh}(f) \le \left(\frac{V^{(I)}\sqrt{\mathrm{Coh}^{(I)}} + V^{(A)}}{V^{(I)} + V^{(A)}}\right)^2. \tag{5}$$

For sufficiently large values of $\Delta_{BR}\sin\alpha$ (distance of the trajectories) the quantity $\mathrm{Coh}^{(I)}$ is small. Consequently, the values of measured coherency can approach 1 provided $V^{(I)} \ll V^{(A)}$. For the model of the spectrum Φ_ν described above, the ratio $V^{(I)}/V^{(A)}$ at low frequencies can be estimated as

$$\frac{V^{(I)}}{V^{(A)}} = \mathrm{const}\frac{\left(\max\left(l_K, \sqrt{\lambda L}\right)\right)^{-4/3}C_K^2}{C_W^2}. \tag{6}$$

The constant in (6) depends on $\cos\alpha$ [*Gurvich and Brekhovskikh*, 2001], but it does not depend on parameters defining the properties of irregularities. It follows from (5) and (6) that large values (close to 1) of measured $\mathrm{Coh}(f)$ at some altitudes for $\Delta_{BR}\sin\alpha > (\max(l_K, \sqrt{\lambda L}))$ indicate the essentially anisotropic nature of irregularities at the corresponding scales. Therefore we can suppose that there is enough stability in the stratosphere at these altitudes to protect the internal waves from breaking and/or the locally isotropic turbulence is weak for breaking the structures created by the internal waves. On the contrary, small values of $\mathrm{Coh}(f)$ indicate that wave breaking and locally appearing isotropic turbulence break down the anisotropic irregularities of wave nature.

[19] These hypotheses based on qualitative consideration require confirmation or quantitative refinement based on experimental data. As follows from the above consideration, high coherency in oblique occultations indicates that the irregularities of the corresponding scales are essentially anisotropic. Therefore we can suppose that the stability is sufficient at these altitudes to prevent or limit the breaking of internal waves and to reduce the occurrence of locally isotropic turbulence. Reciprocally, small values of coherency suggest significant wave breaking and frequent occurrence of isotropic turbulence with an amplitude sufficient to break down the anisotropic irregularities of wave nature.

3. Experimental Results

[20] GOMOS is equipped with two fast photometers sampling simultaneously the star flux with a frequency of 1 kHz at two wavelengths in low-absorption regions: "blue" (470–520 nm, with the central wavelength λ_B = 499 nm) and "red" (650–700 nm, with the central wavelength λ_R = 672 nm). Detailed technical information on the Envisat mission and the GOMOS instrument can be found

Table 1. Characteristics of the Occultation[a]

Number	Orbit	Star	α, °	Tangent Point	Date and Time UT	SMLT	N/S, %	V_P, km/s
V1	2254	α CMa	−2.07	139.9°E, 71.0°S	5 Aug 2002 1423	2343	0.5	3.0
V2	2266	α CMa	−0.11	161.5°W, 70.5°S	6 Aug 2002 1031	2345	0.5	3.0
V3	3057	α PsA	−3.28	80.5°E, 59.1°N	1 Oct 2002 1540	2102	2.0	2.9
V4	3061	α PsA	−3.75	20.3°W, 59.1°N	1 Oct 2002 2223	2102	2.0	2.9
V5	4875	β Car	−0.16	69.4°E, 16.8°N	4 Feb 2003 1717	2154	2.8	2.8
V6	4877	β Car	−0.26	19.0°E, 16.8°N	4 Feb 2003 2039	2155	2.8	2.8
O1	3057	α Car	46.0	113.1°E, 9.8°S	1 Oct 2002 1520	2254	0.6	2.5
O2	3058	α Car	46.1	88.1°E, 9.8°S	1 Oct 2002 1701	2253	0.6	2.5
O3	3059	α Car	46.1	63.0°E, 9.8°S	1 Oct 2002 1840	2252	0.6	2.5
O4	3060	α Car	46.1	37.8°E, 9.8°S	1 Oct 2002 2021	2252	0.6	2.5
O5	3061	α Car	46.1	12.7°E, 9.7°S	1 Oct 2002 2203	2253	0.6	2.5
O6	3062	α Car	46.2	12.5°W, 9.7°S	1 Oct 2002 2342	2252	0.6	2.5
O7	3064	α Car	46.2	62.7°W, 9.7°S	2 Oct 2002 0304	2253	0.6	2.5
O8	3065	α Car	46.2	87.8°W, 9.7°S	2 Oct 2002 0444	2253	0.6	2.5
O9	3067	α Car	46.3	138.1°W, 9.2°S	2 Oct 2002 0806	2254	0.6	2.5

[a]Values of α are given with the correction on the Earth's rotation. SMLT is Solar Mean Local time. N/S is RMS of shot noise to mean signal ratio for altitudes above 90 km.

in ESA web pages http://envisat.esa.int/dataproducts/gomos/CNTR3-1-2.htm#eph.gomos.tgins.insides.ifunc.tphot and http://envisat.esa.int/dataproducts/gomos/CNTR3-2.htm#gomos.tgins.ichper.

[21] The occultations of very bright stars (Table 1) were chosen for the analysis in order to avoid the influence of the instrumental noise. Shot noise to mean signal ratios were less than 1–3% for all observations. Selecting observation events, we aimed first of all at the validation of the theoretical conclusions of section 2 and at studying, in practice, the coherency of two-wavelength scintillations.

[22] In addition to scintillation, the photometer signals also contain slow variations caused by absorption and scattering of the light in the atmosphere and by refractive dilution [*Dalaudier et al.*, 2001]. These effects become more significant as the rays deepen into the atmosphere. In order to remove the slow variations from the signals, they were normalized by their smoothed values obtained by convolving the original signals with a wide Gaussian window. The width of the window (at 1/e level) was 2 s for occultations with small α (Table 1, V1–V6) and 3 s for oblique settings (Table 1, O1–O9). The convolution was computed from the minimal ray perigee altitude up to altitudes (≥100 km) where fluctuations of refractive index are very small. In the following, we considered signals with this normalization applied.

[23] We consider before the examples explaining considered phenomena. Figure 2 shows two short samples of scintillation records for observations V5 and O6. The cross-correlation coefficients of these bi-chromatic scintillations are 0.82 and 0.33, and RMS of the normalized intensity fluctuations are 0.46 and 0.29 for V5 and O6, respectively. This plot demonstrates sharp distinction of scintillation corresponding to different coherency extent. It is necessary to note that we cannot perform in practice the synchronous observations in the same place with different angles α. Therefore the noted difference scintillation characteristics may be related not only to the difference in angles α.

[24] The time-frequency analysis [*Flandrin*, 1999] was applied for study of the scintillation coherency. Each normalized record corresponding to one occultation was divided into intervals of the same duration T_0 depending on angle α with overlapping by $T_0/4$. For each interval, the auto-spectra $V_B(f_i;t_j)$, $V_R(f_i;t_j)$ and cross-spectrum $V_{BR}(f_i;t_j)$ (f_i is the discretized frequency) were calculated. The moments t_j, j = 1, 2, ... corresponding to the midpoint of each interval are the second argument of the time-frequency spectrum. The estimates of spectral densities were calculated by smoothing the periodogram obtained by FFT. We used a Hanning window [*Oppenheim and Schafer*, 1989] for the smoothing. The central frequency of the most low-frequency window f_1 was always $f_1 = 3/T_0$. The width of this window was also $3/T_0$. The width of each subsequent window increases by $2/T_0$, while its central frequency coincides with the upper frequency bound of the previous one. Thus the width of the spectral window progressively increases with growing frequency. The frequency grid is chosen in such a way as to give better smoothing at high frequencies and preserve the

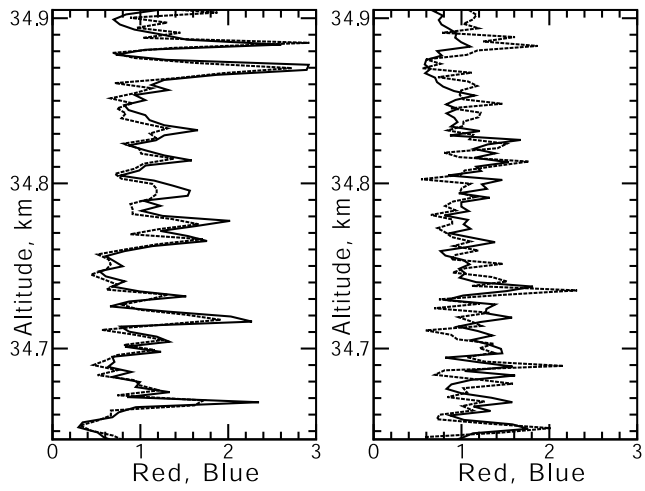

Figure 2. Comparison of two records of two-wavelength scintillations ((left) vertical V5, (right) oblique O6). Abscissa is red (dashed line) and blue (solid line) intensities normalized on the corresponding mean. Ordinates are altitude of ray perigee. The altitude of the curve for blue photometer was shifted 5 m downward in order to compensate for the calculated chromatic shift Δ_{BR}.

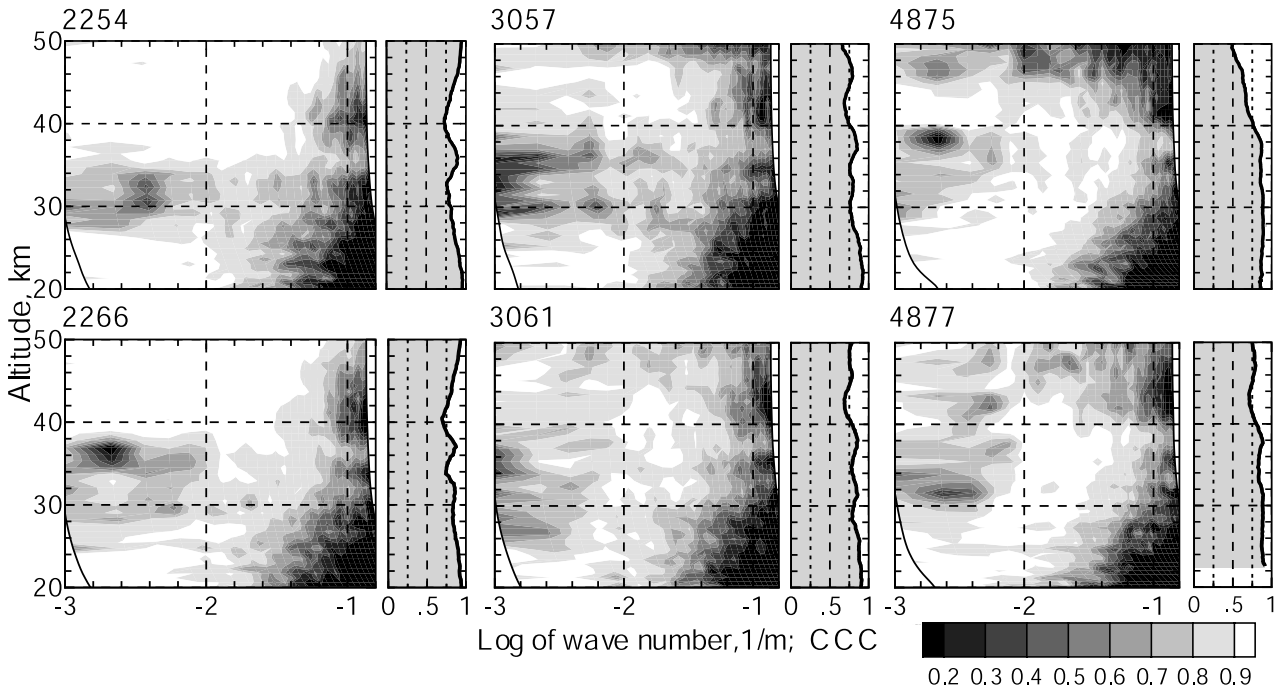

Figure 3. Close to vertical star set observations V1–V6. Estimates of coherency $\mathrm{Coh}_{i,j}$ (columns 1, 3, and 5) and correlation coefficients CCC (columns 2, 4, and 6). Orbit number appears above each plot. See color version of this figure at back of this issue.

necessary spectral resolution at low frequencies. We calculated coherence spectra by using

$$\mathrm{Coh}_{i,j} = \mathrm{Coh}(f_i, h_j) = \frac{|V_{BR}(f_i, h_j)|^2}{V_B(f_i, h_j) V_R(f_i, h_j)}. \quad (7)$$

[25] The ray perigee altitude h_j corresponding to each value t_j was taken as the same for blue and red rays. The variance profiles of normalized red and blue scintillations were close, taking into account the influence of optical band.

[26] We had chosen the altitude range 20–50 km because of the following reasons. The chromatic refraction effects above 50 km are too weak for observations from Envisat orbit. Below 20 km, the recorded photometer signals weaken significantly because of absorption and scattering in the atmosphere. Fluctuations of absorption and scattering coefficients, in turn, may result in additional low-frequency variations in the recorded signals. Furthermore, the strong scintillations appear at altitudes 22–25 km [*Gurvich et al.*, 2001]. Under these conditions, the assumption on statistical independence of scintillations induced by isotropic and anisotropic part of the 3-D spectrum of irregularities may be violated.

[27] For overall integral characterization of coherency, we used the cross-correlation coefficient CCC of the signals of the blue and the red photometers, defined as a maximum of the cross-correlation function CCF(τ) of these two signals,

$$CCF(\tau) = \frac{\langle (B(t) - \bar{B}(t))(R(t+\tau) - \bar{R}(t+\tau)) \rangle}{\sqrt{\left\langle (B - \bar{B})^2 \right\rangle} \sqrt{\left\langle (R - \bar{R})^2 \right\rangle}}, \quad (8)$$

where $B(t)$ and $R(t)$ are the records of blue and red photometers. In our processing, the red signal was shifted of the estimated time delay τ_A [*Dalaudier et al.*, 2001; *Kan et al.*, 2001]. Such processing guarantees that the maximum of the cross-correlation function is achieved in the vicinity of zero lag; therefore, the cross-correlation coefficient can be expressed in terms of spectral densities as

$$CCC \approx \frac{\int \mathrm{Re}\{V_{BR}(f)\} df}{\sqrt{\int V_B(f) df} \sqrt{\int V_R(f) df}}. \quad (9)$$

The cross-correlation coefficient may be therefore considered as an integral characteristic of coherency.

[28] The correlation coefficient was calculated at sampling frequency 40 Hz; that is, the central points of each sample are separated by 25 ms. The length of the samples corresponds to 250 m motion of tangent point. The signal of the red photometer was pre-shifted for the estimated time delay. Additionally, the red signal was smoothed by a Gaussian window (of variable length, depending on altitude) in order to "equate" the refractive smoothing of both signals. The obtained values of the correlation coefficients were smoothed afterward for better appearance, so that the vertical resolution of CCC profiles presented in Figures 3 and 4 corresponds to $\sim$1 Hz.

[29] Examples of the coherency Coh for occultations close to vertical are shown in Figure 3 as a functions of two variables: altitude and vertical wave number f/V_P where $V_P = V_S \cos \alpha$ is vertical velocity of ray perigee point. The values of V_P for the ray perigee altitude of 30 km are given in Table 1. Values of α in this table are given with the

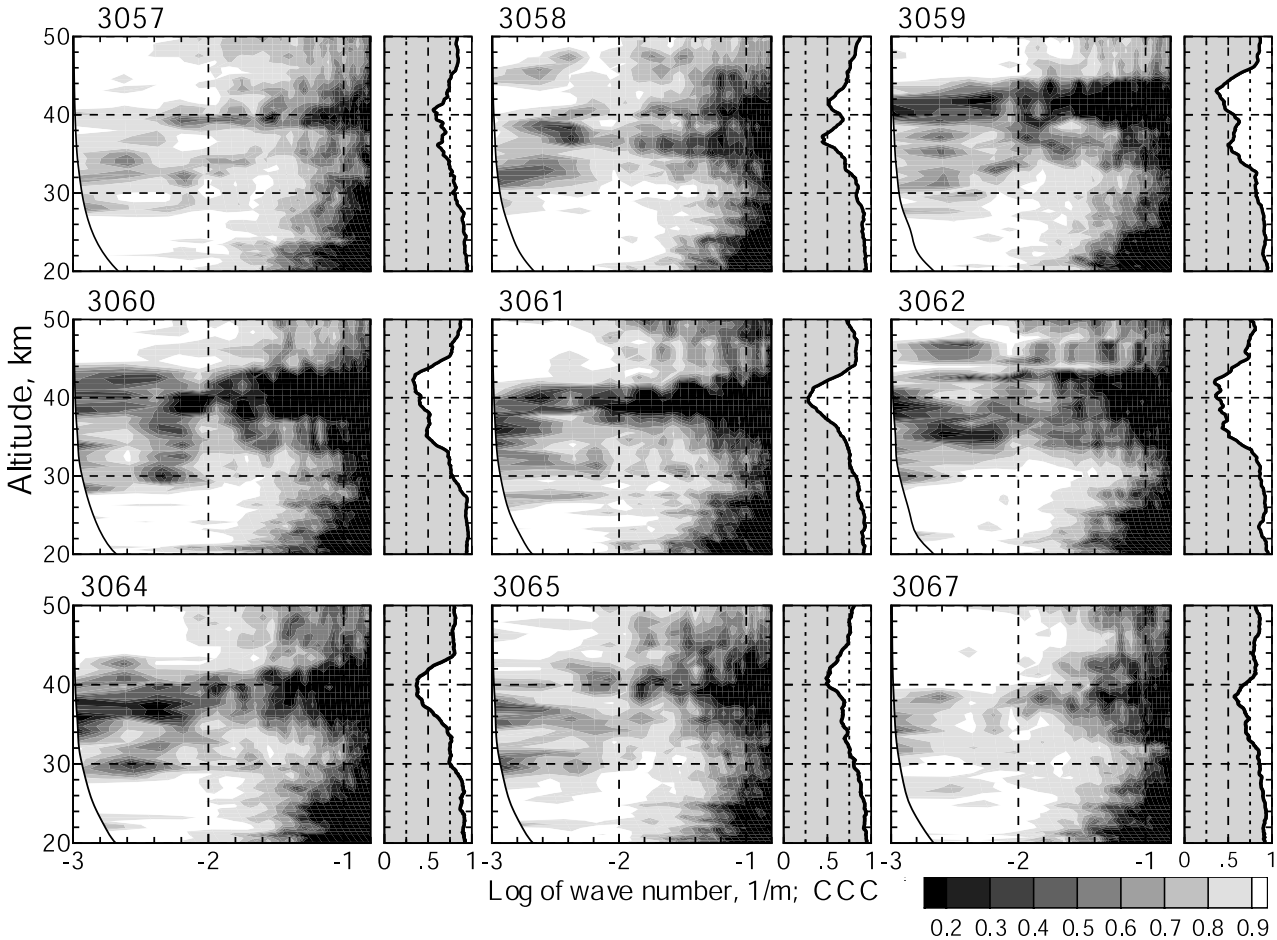

Figure 4. Oblique star set observations O1–V9. Estimates of coherency $Coh_{i,j}$ (columns 1, 3, and 5) and correlation coefficient CC (columns 2, 4, and 6) obtained from observations with large angles α. Orbit number appears above each plot. See color version of this figure at back of this issue.

correction for the Earth's rotation. SMLT is Solar Mean Local Time. N/S is the ratio of RMS shot noise to mean signal above the atmosphere for ray perigee altitudes more than 90 km.

[30] The time intervals $T_0 = 1.024$ s were used in the data processing. Velocities V_P for the observations of Figure 3 coincide practically with V_S because cos α is close to 1 for these observations. The logarithmic scale for wave number on the plot of Figure 3 allows better visibility at low frequencies or, equivalently, at large scales. We took into account the rotation of the Earth in computing α for observations V1–V6. This may be especially important for small angles α. The areas of high coherency dominate in Figure 3, as it was predicted by the qualitative theory. However, there are areas of decreased coherency. The coherency reduction at lower altitudes ($h < 25 \div 30$ km) and for small scales $V_P/f < 10 \div 30$ m is not surprising. This may be the result of the averaging of scintillations over the wavelength bands of optical filters of photometers [*Kan et al.*, 2001; *Gurvich and Brekhovskikh*, 2001]. The estimates of Δ_R and Δ_B given in section 2 show that the difference in the spatial averaging will distort the scintillations of blue and red rays at altitudes below 30 km. As a consequence, the coherency of the observed scintillations may be reduced. Furthermore, the high-frequency scintillations with a scale <10 m are induced by locally isotropic turbulence [*Gurvich and Kan*, 2003b]. Therefore the coherency reduction at high spatial frequencies log $(f/V_P) > -1$ is observed in Figure 3 for all altitudes. Additionally, light scattering and refractive dilution at lower altitudes attenuate the stellar signal. This also results in decreased coherency.

[31] The coherency reduction at low wave numbers log $(f/V_P) < -2 \div -2.5$ at altitudes 25–40 km in Figure 3 looks at first surprising. From our point of view, this effect could be related to the outer scale of the anisotropic irregularities [*Gurvich and Chunchuzov*, 2005]. The outer scale bounds their spectrum for large scales.

[32] Figure 4 shows the results of the coherency analysis for oblique occultations. The successive occultations of the very bright star Canopus (α Car) were performed on 1–2 October 2002. Table 1 contains additional information about these observations. Note that all these observations were performed nearly at the same local time; they are located at approximately the same latitude and cover the corresponding zone.

[33] The time interval $T_0 = 1.024$ s was used in data processing of oblique occultations. For presentation of these data we chose wave number f/V_P where $V_P = V_S \cos \alpha$. This wave number is more convenient than f/V_S for description of scintillations caused by irregularities stretched along the

Earth's surface. Specifically, such irregularities define a region of high coherency.

[34] The coherency of scintillations generated by isotropic irregularities should decrease with growth of α, as is predicted by the qualitative considerations in section 2. This is clearly seen from comparison of CCC profiles in Figures 3 and 4. Hence, according to (5), the regions where scintillations are generated by anisotropic irregularities should be detected more clearly. The coherency maps in Figure 4 demonstrate this.

[35] First of all, the existence of layers with low coherency can be noticed in most panels in Figure 4. These layers are especially visible for orbits 3059–3064, where the low coherency is observed for all wave numbers. The isotropic irregularities have a dominant role in the region between 60°E and 60°W into some zone around 9.7°S at altitudes 35–43 km. We may assume that breakdown of inner gravity waves was strongly pronounced in that layer.

[36] The reduction in coherency with increasing wave number outside these layers is more noticeable in Figure 4 than in Figure 3. Note that this happens at those wave numbers where, as estimates Δ_R and Δ_B show, the influence of the averaging caused by different wavelength bands of optical filter of photometers is insignificant. Such behavior of coherency is related to the weakening of the spectrum of anisotropic irregularities at wave numbers close to buoyancy scale [*Gurvich and Kan*, 2003b; *Gurvich and Chunchuzov*, 2003] and larger. The scintillations with large wave numbers are dominated by locally isotropic irregularities [*Gurvich and Brekhovskikh*, 2001]. However, the coherency of scintillations generated by the isotropic irregularities is low under observation conditions as in Figure 4 (large values of $\alpha > \alpha_{\max}$). Therefore the coherency presented in Figure 4 gives the qualitative dependence of buoyancy scale upon altitude outside the regions where coherency is low at all frequencies.

[37] It is interesting to notice the reduction of coherency for some occultations at altitudes 30–35 km and at wave numbers <0.01 m^{-1}. It can be explained, from our point of view, by degradation of large-scale anisotropic irregularities at these altitudes. In other words, it can be interpreted in terms of the outer scale of the anisotropic irregularities in the stratosphere [*Gurvich and Chunchuzov*, 2005].

[38] Comparison of the coherency and profiles of CCC show that the latter is a convenient and simple parameter for characterizing coherency of two-wavelength scintillations for angles α significantly different from zero. For α close to zero the values of this parameter have weaker variations. Using this parameter opens a possibility for mapping the ratio of anisotropic and isotropic irregularities of air density.

[39] Altitude dependence of coherency and profiles of cross-correlation coefficient is in qualitative agreement with the current theory of the IGW propagation [*Fritts and Alexander*, 2003; *Sutherland*, 2001]: They propagate upward with increasing amplitude (caused by decreasing air density) until they reach instability conditions and break down. The turbulence, appearing from the breaking of IGW, leads to effective turbulent mixing of the stably stratified stratosphere and to dissipation of kinetic energy into heat at the final step of this process.

[40] The appearance of locally isotropic turbulence on wave trajectories leads, as is mentioned above, to reduction in coherency of bi-chromatic scintillations. At altitudes above 45–50 km, the chromatic separation of rays becomes too small, so that it is impossible to observe the appearance of the locally isotropic turbulence, even if it exists.

4. Conclusions

[41] The scintillations of stars observed through the Earth's atmosphere are generated by random irregularities of the air density. In this paper, we propose a qualitative theory for the description of the coherency of optical scintillations measured at two wavelengths.

[42] The theoretical approach is based on two-component model of the air density irregularities. It is assumed that one of the components is generated by locally isotropic turbulence. The second, anisotropic one is a consequence of the internal gravity waves activity. The main conclusion of the developed theory is that chromatic aberration degrades the coherency of scintillations generated by isotropic irregularities. The largest decrease in coherency should be observed in oblique occultations.

[43] The scintillations at two wavelengths measured by GOMOS FP on board the Envisat satellite have confirmed the theoretical conclusions. The analysis has been performed for the altitude range 20–50 km. Synchronous observations of scintillations at two wavelengths $\lambda_R = 672$ and $\lambda_B = 499$ nm have allowed the detection of layers with prevailing isotropic component. They are located generally between the altitudes of about 30 and 40 km. The thickness of the layers and their altitude distribution depend on observation location. It can be assumed that the locally isotropic turbulence is well developed within these layers.

[44] The coherency computed from the scintillation data visualizes the regions of high and low coherency. Anisotropic irregularities dominate in the high-coherency regions. The altitude dependence of the characteristic wave numbers corresponding to buoyancy scales can be observed within these regions. The wave number corresponding to the outer scale in the spectrum of anisotropic irregularities can sometimes be detected. We can assume that these scales correspond to an outer scale in the gravity wave spectrum. It may be assumed that the stability conditions for IGW are reduced somehow in the low-coherency regions and that the breakdown of waves generates locally isotropic turbulence.

[45] It was shown that the low values of the maximum of the cross-correlation function of two-wavelength scintillations can be used as a qualitative indicator for the presence of layers with prevailing isotropic turbulence.

[46] The obtained results show that the analysis of coherency of the two-wavelength scintillations in the stratosphere is a new approach which allows separate study of the locally isotropic density irregularities and the ones stretched along the Earth's surface. Further analysis of the GOMOS FP data will give us information about global distribution and magnitude of the stratospheric layers with high intensity of isotropic turbulence.

Appendix A: Estimations of Ray Divergence for Vertical Occultations

[47] Let us consider the limit case $\alpha = 0$. In this case, both rays are in the same plane $y = 0$ (Figure 1), while the

observation point moves along this plane. The tangent altitude $h_B(t)$ of the blue ray at the moment $t = t_0 + \delta\tau$, $\delta\tau = \Delta_{BR}/V_S$ is equal to the tangent altitude $h_R(t_0)$ of the red ray at the moment $t = t_0$. Nevertheless, the rays with $h_R(t_0) = h_B(t_0 + \delta\tau)$ do not coincide (Figure 1, top) because of the difference $\delta\varepsilon_{BR}$ in refractive angles ε: $\delta\varepsilon_{BR} = \varepsilon_B(h_R(t_0)) - \varepsilon_R(h_R(t_0 + \delta\tau))$. Besides, the curvature of the blue ray is larger than that of the red ray. The noncoincidence of ray trajectories is the main reason for coherency reduction for small $\alpha \simeq \alpha_{max}$ or less.

[48] The effective divergence of the rays in the atmosphere can be estimates by the value of $\delta\varepsilon_{BR}L_A/2$, where $L_A = \sqrt{2H_0a_E}$ is an effective path of interaction between a ray and the atmosphere, H_0 is the atmospheric characteristic scale at a ray perigee altitude, and a_E is the Earth's radius. At the ray perigee altitude 30 km, the effective divergence is ~0.9 m. Consequently, even in exactly vertical occultation ($\alpha = 0$), the dependence of refractive angle on wavelength can significantly reduce the coherency of isotropic scintillations observed at two wavelengths.

[49] The second reason for coherency reduction of isotropic scintillations is the rotation of the atmosphere together with the Earth with respect to stars and, consequently, to the orbital plane [*Dalaudier et al.*, 2001]. If $\alpha = 0$, then the observed star is in the orbital plane. The inclination of the Envisat orbit is 98.6°. If the observed star is located far away from the celestial equator, then the ray perigee altitude is near to the terrestrial equator. During time $\delta\tau$, the irregularities located at the altitude $h_R(t_0)$ at the moment t_0 will displace almost along the perpendicular to the ray, which belongs to the plane $y = 0$. This displacement can be estimated by the value $\omega a_E\delta\tau \cos\beta$, where ω is the angular velocity of the Earth's rotation, $\omega a_E = 470$ m/s, and β is the star declination. The velocity V_P decreases accordingly as the ray perigee goes down in the atmosphere [*Dalaudier et al.*, 2001, Figure 2]. At the ray perigee altitude 30 km, $V_P \cong 2.8$ km/s [*Dalaudier et al.*, 2001]. Thus the displacement caused by the Earth's rotation can be estimated as 1.7 cos β meters. For some values of α the Earth's rotation can be compensated, but the compensation conditions are satisfied only at some altitude ranges, because of vertical velocity V_P depends on ray perigee altitude.

[50] **Acknowledgments.** The work was supported by RFBR grant 03-05-64366 and CNRS-RAS collaboration project 16340. The authors thank the GOMOS CAL/VAL team.

References

Alexandrov, A. P., G. M. Grechko, A. S. Gurvich, V. Kan, M. K. Manarov, A. I. Pakhomov, Y. V. Romanenko, S. A. Savchenko, C. I. Serova, and V. G. Titiov (1990), Temperature spectra in the stratosphere from observations of star scintillations from space, *Izv. Atmos. Oceanic Phys.*, *26*, 1–8.

Dalaudier, F., V. Kan, and A. S. Gurvich (2001), Chromatic refraction with global ozone monitoring by occultation of stars: I. Description and scintillation correction, *Appl. Opt.*, *40*, 866–877.

Elliot, J. L., and J. Veverka (1976), Stellar occultation spikes as probes of atmospheric structure and composition, *Icarus*, *27*, 359–386.

Flandrin, P. (1999), *Wavelet Analysis and its Applications*, vol. 10, *Time-Frequency/Time-Scale Analysis*, Elsevier, N. Y.

Fritts, D. C., and M. J. Alexander (2003), Gravity waves dynamics and effects in the middle atmosphere, *Rev. Geophys.*, *41*(1), 1003, doi:10.1029/2001RG000106.

Fritts, D. C., and T. E. VanZandt (1993), Spectral estimates of gravity wave energy and momentum fluxes: Part 1. Energy dissipation, acceleration, and constraints, *J. Atmos. Sci.*, *50*, 3685–3694.

Gurvich, A. S. (2002), Parameters of turbulence and internal waves and the dissipation of kinetic energy in the stratosphere based on space observations, *Dokl. Earth Sci.*, *385*, 599–603.

Gurvich, A. S., and V. L. Brekhovskikh (2001), Study of the turbulence and inner waves in the stratosphere based on the observations of stellar scintillations from space: A model of scintillation spectra, *Waves Random Media*, *11*, 163–181.

Gurvich, A. S., and I. P. Chunchuzov (2003), Parameters of the fine density structure in the stratosphere obtained from spacecraft observations of stellar scintillations, *J. Geophys. Res.*, *108*(D5), 4166, doi:10.1029/2002JD002281.

Gurvich, A., and I. Chunchuzov (2005), Estimates of characteristic scales in the spectrum of internal waves in the stratosphere obtained from space observations of stellar scintillations, *J. Geophys. Res.*, *110*, D03114, doi:10.1029/2004JD005199.

Gurvich, A. S., and V. Kan (2003a), Structure of air density irregularities in the stratosphere from spacecraft observations of stellar scintillation: 1. Three-dimensional spectrum model and recovery of its parameters, *Izv. Atmos. Oceanic Phys.*, *39*, 300–310.

Gurvich, A. S., and V. Kan (2003b), Structure of air density irregularities in the stratosphere from spacecraft observations of stellar scintillation: 2. Characteristic scales, structure characteristics, and kinetic energy dissipation, *Izv. Atmos. Oceanic Phys.*, *39*, 311–321.

Gurvich, A. S., et al. (2001), Studying the turbulence and inner waves in the stratosphere with spacecraft observations of stellar scintillation: I. Experimental technique and analysis of the scintillation variance, *Izv. Atmos. Oceanic Phys.*, *37*, 436–451.

Hubbard, W. B., et al. (1993), The occultation of 28 Sgr by Titan, *Astron. Astrophys.*, *269*, 541–563.

Ishimaru, A. (1978), *Wave Propagation and Scattering in Random Media*, vol. 2, Elsevier, New York.

Kan, V. (2004), Coherence and correlation of chromatic stellar scintillations in a spaceborne occultation experiment, *Atmos. Oceanic Opt.*, *17*, 725–735.

Kan, V., F. Dalaudier, and A. S. Gurvich (2001), Chromatic refraction with global ozone monitoring by occultation of stars: II. Statistical properties of scintillations, *Appl. Opt.*, *40*, 878–889.

Kyrölä, E., et al. (2004), GOMOS on Envisat: An overview, *Adv. Space Res.*, *33*, 1020–1028, doi:10.1016/S0273-1177(03)00590-8.

Oppenheim, A. V., and R. W. Schafer (1989), *Discrete-Time Signal Processing*, Prentice-Hall, Upper Saddle River, N. J.

Sutherland, B. R. (2001), Finite-amplitude internal wavepacket dispersion and breaking, *J. Fluid Mech.*, *429*, 343–380.

Tatarskii, V. I. (1971), *The Effects of the Turbulent Atmosphere on Wave Propagation*, 417 pp., U.S. Dep. of Commer., Springfield, Va.

F. Dalaudier, Service d'Aeronomie, Paris, France. (francis.dalaudier@aerov.jussieu.fr)

A. S. Gurvich, A. M. Oboukhov Institute of Atmospheric Physics, Pyzhevsky 3, Moscow 119017, Russia. (gurvich@ifaran.ru)

V. F. Sofieva, Finnish Meteorological Institute, Helsinki, Finland. (viktoria.sofieva@fmi.fi)

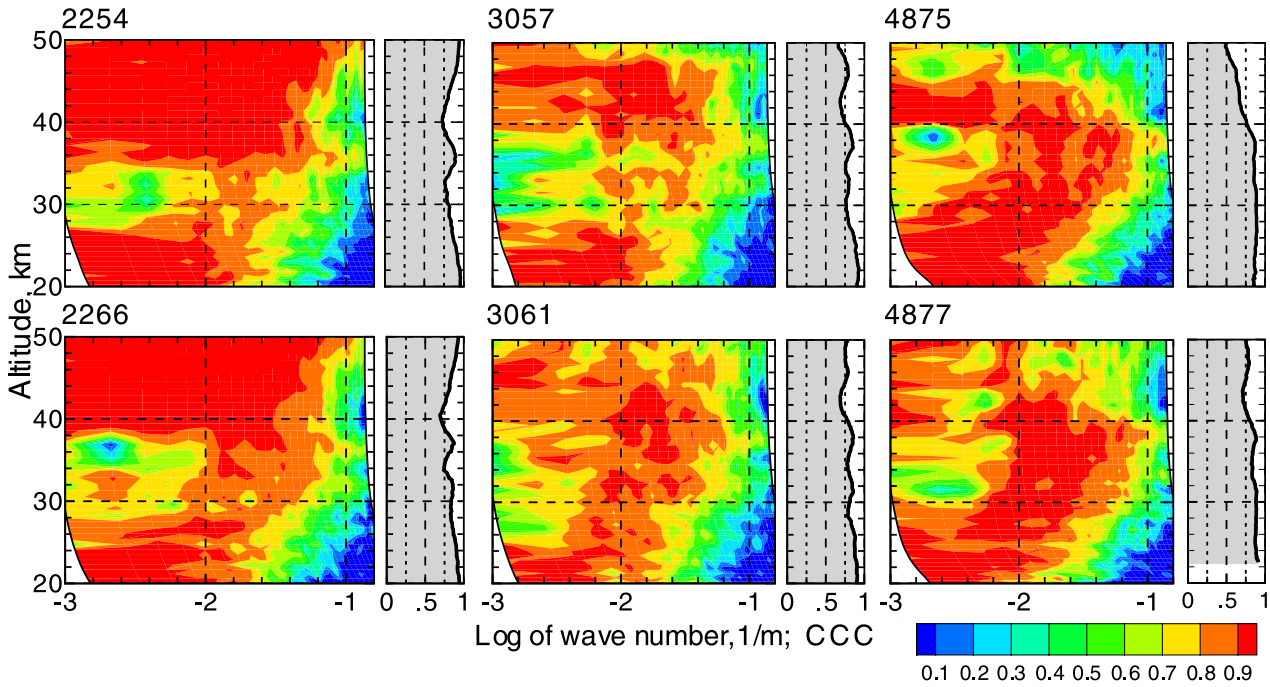

Figure 3. Close to vertical star set observations V1–V6. Estimates of coherency $Coh_{i,j}$ (columns 1, 3, and 5) and correlation coefficients CCC (columns 2, 4, and 6). Orbit number appears above each plot.

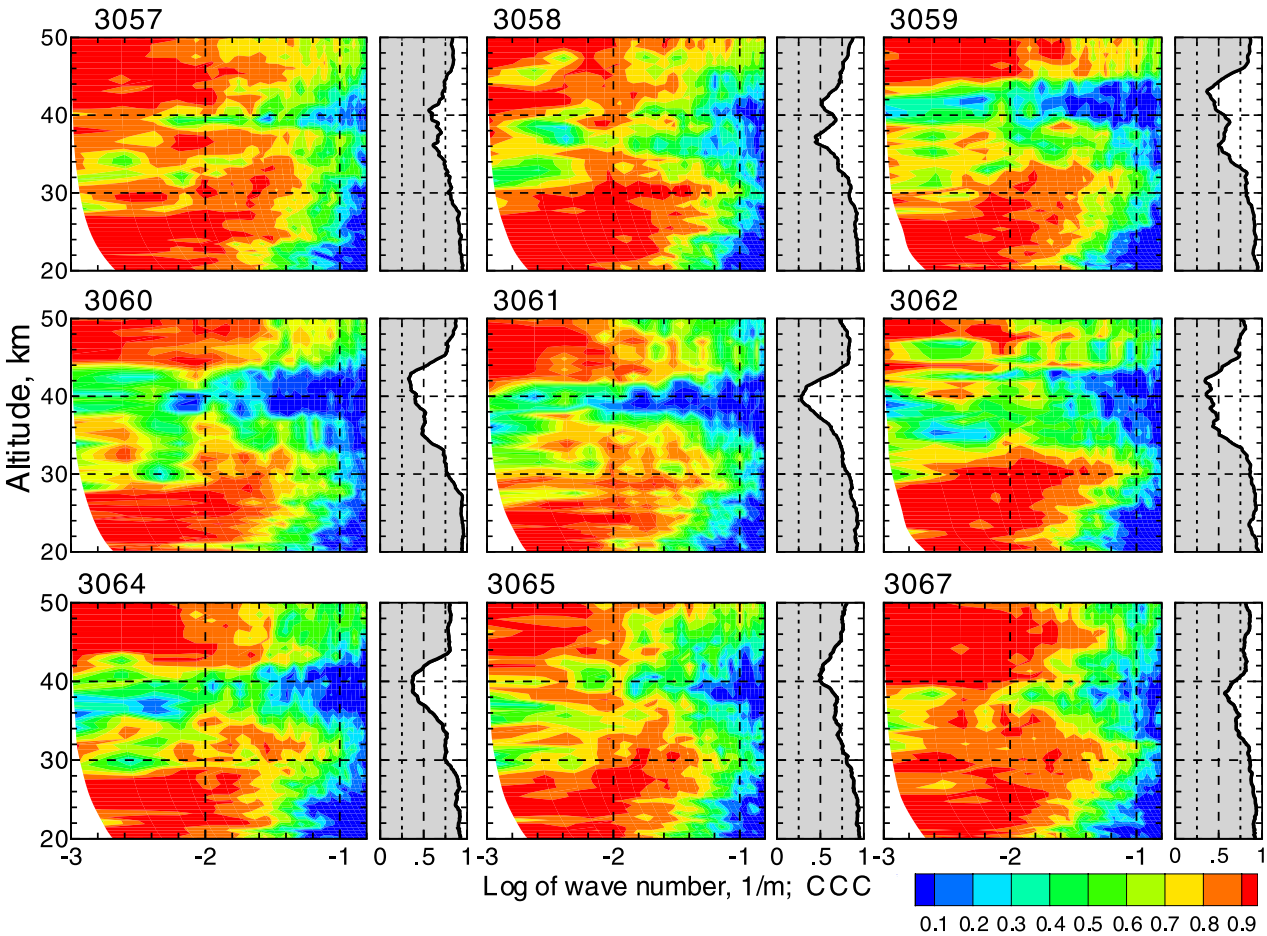

Figure 4. Oblique star set observations O1–V9. Estimates of coherency $Coh_{i,j}$ (columns 1, 3, and 5) and correlation coefficient CC (columns 2, 4, and 6) obtained from observations with large angles α. Orbit number appears above each plot.